Journal of Marine Science and Technology

Volume 32 | Issue 2 Article 7

Analysis of the Potential for Enhancing the Efficiency of a Floating Photovoltaic (FPV) System

How-Ping Wu
Department of Mechanical Engineering, National Taiwan University, No. 1, Sec. 4, Roosevelt Road, Taipei, 10617, Taiwan.

Ching-Yi Tseng
Department of Mechanical Engineering, National Taiwan University, No. 1, Sec. 4, Roosevelt Road, Taipei, 10617, Taiwan., d04522010@ntu.edu.tw

Chuan-Chung Jen
Department of Mechanical Engineering, National Taiwan University, No. 1, Sec. 4, Roosevelt Road, Taipei, 10617, Taiwan.

Yuan-Ching Chiang
Department of Mechanical Engineering, Chinese Culture University, No. 55, Hwa-Kang Road, Yang-Ming-Shan, Taipei, 11114, Taiwan.

Sih-Li Chen
Department of Mechanical Engineering, National Taiwan University, No. 1, Sec. 4, Roosevelt Road, Taipei, 10617, Taiwan.

Recommended Citation

Wu, How-Ping; Tseng, Ching-Yi; Jen, Chuan-Chung; Chiang, Yuan-Ching; and Chen, Sih-Li (2024) "Analysis of the Potential for Enhancing the Efficiency of a Floating Photovoltaic (FPV) System," *Journal of Marine Science and Technology*: Vol. 32: Iss. 2, Article 7.
DOI: 10.51400/2709-6998.2740
Available at: https://jmstt.ntou.edu.tw/journal/vol32/iss2/7

RESEARCH ARTICLE

Analysis of the Potential for Enhancing the Efficiency of a Floating Photovoltaic (FPV) System

How-Ping Wu [a], Ching-Yi Tseng [a,*], Chuan-Chung Jen [a], Yuan-Ching Chiang [b], Sih-Li Chen [a]

[a] Department of Mechanical Engineering, National Taiwan University, No. 1, Sec. 4, Roosevelt Road, Taipei, 10617, Taiwan
[b] Department of Mechanical Engineering, Chinese Culture University, No. 55, Hwa-Kang Road, Yang-Ming-Shan, Taipei, 11114, Taiwan

Abstract

This study examined the power generation capabilities of FPV systems and the advantages of employing active cooling on floating solar panels. Floating solar panels exhibit improved efficiency due to operating at lower temperatures facilitated by the cooling effect of water evaporation. Additionally, the high availability of water renders the application of the active cooling technique economically viable. This study developed a comprehensive simulation of a floating solar system, integrating a mathematical model to validate experimental findings and a temperature model derived from an energy equation specific to floating solar panels. This model calculates the heat transfer among the three different materials in the solar panels and accounts for various boundary conditions. This model exhibits better accuracy performance than other temperature models, such as the NOCT or the lumped system model. Notably, it demonstrates a lower root-mean-square error (RMSE) of 0.97 °C in the passive cooling mode, 2.36 °C in the water film cooling mode, and 1.71 °C in the water spray cooling mode. Therefore, this model effectively predicts solar panels' surface temperature for different cooling methods. The experimental results demonstrate that floating solar panels maintain an average temperature of 4 °C lower than rooftop solar panels, resulting in a 3.27% power increase. With water film cooling, the average temperature decreased by 19.39 °C than without water cooling, leading to a 6.70% increase in power generation. After deducting the energy consumption of the cooling system, the net energy gain reached 5.27%. Similarly, with water spray cooling, the average temperature decreased by 16.29 °C, resulting in a 6.38 increase in power generation, with a net energy gain of 3.93%.

Keywords: Floating solar photovoltaic system, Active cooling on solar panels, Solar panel efficiency enhancement, Optimized operating temperature of active cooling

1. Introduction

Photovoltaic (PV) solar energy is one of the most developed renewable energies globally, with different studies conducted worldwide [1]. Its development primarily focuses on cost reduction and performance improvement. Solar energy development is categorized into four generations, which have been initially helpful in navigating the complex PV landscape [2]. Additionally, many installations are situated on reservoirs or lakes [3]. Ensuring the structural integrity and longevity of the foundation is crucial for the safe and dependable installation of water [4]. To address land use limitations, floating solar systems emerged as a popular solution for PV installations [5]. Beyond land constraints, elevated cell temperatures pose another challenge for PV panels, as semiconductor performance diminishes with rising module temperature. FPV systems mitigate this issue by achieving lower cell temperature and exhibiting a 5%−15% higher efficiency than land-based PV systems, attributed to the cooling effect of water evaporation [6]. Choi [7] compared 100 kW and

Received 3 December 2023; revised 9 May 2024; accepted 1 June 2024.
Available online 11 July 2024

* Corresponding author.
E-mail address: d04522010@ntu.edu.tw (C.-Y. Tseng).

https://doi.org/10.51400/2709-6998.2740

500 kW FPV systems with a 1 MW land-based PV system under similar weather conditions. Based on a one-year data collection, the average cell temperature of the floating solar panels experienced a significant reduction, leading to an increased conversion efficiency of up to 13.5%. Umoette [8] developed a mathematical model to assess the power gain of PV panels on both on- and offshore installations. Weather data, including temperature and wind speed from Ibeno Beach, were utilized to estimate FPV power generation. Due to an 8% lower ambient temperature and a 67% higher wind speed, the FPV system exhibited lower module temperatures and increased power generation by 4%.

The high availability of water makes other water-cooling techniques economically viable. Several studies have explored different cooling methods for floating solar panels, with two common modes being active cooling and passive cooling [9]. Azmi [10] devised a heat sink attached to the back of floating solar panels in direct contact with the water surface. Exposed to a steady radiation level of 834W/m2 in the laboratory, the floating solar panels demonstrated a 14.55% increase in power output through the heat sink after a 1-hour experiment. Cazzaniga [11] developed a floating tracking cooling concentrating system, incorporating a single-axis solar tracking system, a water film cooling method, and a concentrating technique to the FPV system. The study revealed that the cooling method yielded a net power output increase of 5%. Nisar [12] conducted experiments exploring the tilting effect on FPV panels. They discovered that FPV panels achieved maximum power output when installed at the annual optimal tilting angle. Moreover, the power output of on-ground PV systems was 20−28% lower than FPV systems under varying tilting conditions.

To enhance energy output, researchers have explored various methods to reduce the cell temperature of solar panels. One widely utilized approach is the active water-cooling method, which can be further classified into water spray on the back and water film on the front. Water film cooling facilitates uniform solar panel temperature reduction, leveraging water's high cooling capacity to dissipate heat rapidly. Dorobantu [13] conducted a water film cooling experiment on solar panels, revealing a uniform temperature cooling of about 20 °C, resulting in a 9.5% power increase. Another water-cooling method involves spraying water over the rear side of panels. Despite its low cooling capacity, water spray consumes only a small amount of water while effectively cooling a large surface. Nizetic [14] designed a water spray experiment to compare cooling effects on the front side, back side, and both sides of solar panels. The results indicated that while water spray on the front side yielded a better cooling effect, the droplets blocked solar irradiance, leading to a low power output. Conversely, water spray on the back side demonstrated better efficiency despite the high thermal resistance of the back sheet. Optimal efficiency was achieved with water spray on both sides, resulting in a 5.9% power increase.

To evaluate the temperature impact on solar panels, researchers have examined the relationships between cell temperature and environmental factors, employing mathematical models derived from empirical equations or thermal analysis methods. Akhsassi [15] compared the empirical relations from several studies with experimental weather data. The relations considering wind speed demonstrated a better RMSE accuracy of 1.13−2.03 °C, whereas those without the wind speed factor have a 1.57−3.85 °C RMSE. The transient temperature model of solar panels can be derived by energy equations accounting for thermal mass. Jones [16] modeled solar panels as a lumped system, formulating an ordinary differential equation (ODE) using an energy equation. By calculating the heat convection and radiation between the panels and the surroundings, the model can fit the temperature fluctuation in rapidly changing weather conditions. Hameed [17] also applied energy equations to a 3D transient temperature model, solving them using a finite element method. The temperature distribution in the solar panels included maximum values in the middle of the front panels while the heat was transferred from the front side to the back side. Notton [18] developed a temperature model dividing solar panels into three material-based segments, employing three energy equations to solve a simultaneous equation system, achieving high accuracy (RMSE of 1.3 °C) with experimental data. This model considered the temperature difference between the front and back sides and the properties of different materials.

This study performed a theoretical analysis of PV panels to investigate PV cells under different conditions. The experiments were conducted in a subtropical region, facilitating comparison with studies conducted in diverse climates. Theoretical analysis validated the applicability of FPV in real-world environments.

2. Mathematical models

The thermal analysis of PV panels can be viewed as an inclined plane to evaluate heat conduction across different material layers, heat convection

transfer with air or water cooling on the surface, and heat radiation exchange with the environment. To examine the mathematical models utilizing energy conservation equations, the following assumptions were made:

(1) Heat transfer on the narrow side can be neglected due to their significantly smaller surface area.
(2) The heat generated by the internal resistance of the PV panels can be discounted in the analysis.
(3) The temperature of the cooling water in the tank is assumed to be uniform and constant at 25 °C.
(4) The properties of the materials comprising the panels are assumed to be isotropic and independent of temperature variations.
(5) The temperature distribution within each layer of the solar panels is assumed to be uniform.
(6) Cooling water is assumed to be sprayed evenly onto the panels.
(7) The water film resulting from the cooling process is assumed to be uniform and to flow smoothly over the panels.

2.1. Temperature models of PV panels

The schematic diagram and the thermal resistance model depicted in Fig. 1 illustrate the various heat transfer mechanisms considered in the mathematical model. Here, T_{amb} represents the ambient temperature, T_{sky} represents the sky temperature, and R denotes the heat resistance. Footnotes represent different types of heat transfer: "free" indicates natural convection, "r" signifies radiation, and "forced" represents forced convection. Moreover, footnotes "f," "b," "pv," and "ground" correspond to the front plate, back plate, pv panel, and ground, respectively. Nodes on the thermal resistance diagram indicate temperature T, thermal mass C, and solar radiation Φ.

Sky temperature is a parameter relevant to longwave radiation. Asdrubali et al. [19] leveraged TRNSYS and various models to establish relationships between sky temperature and other parameters. However, due to the unavailability of climate data, ISO13790 [20] suggests deriving sky temperature from ambient temperature by subtracting 13 from the ambient temperature in tropical areas, resulting in a sky temperature of 20 °C in this study.

The heat source for PV panels originates from the solar radiation absorbed by the front glass and the solar cell. A portion of this energy is converted into an electrical output, while the remaining energy dissipates as heat. Heat transfer occurs among different materials via conduction and dissipates to the environment through convection and radiation. By formulating energy conservation equations for each layer of the PV panels, three equations are derived. Given that these equations are time-dependent differential equations, this study employed a second-order midpoint method to solve the ODEs. Experimental data validated the temperature

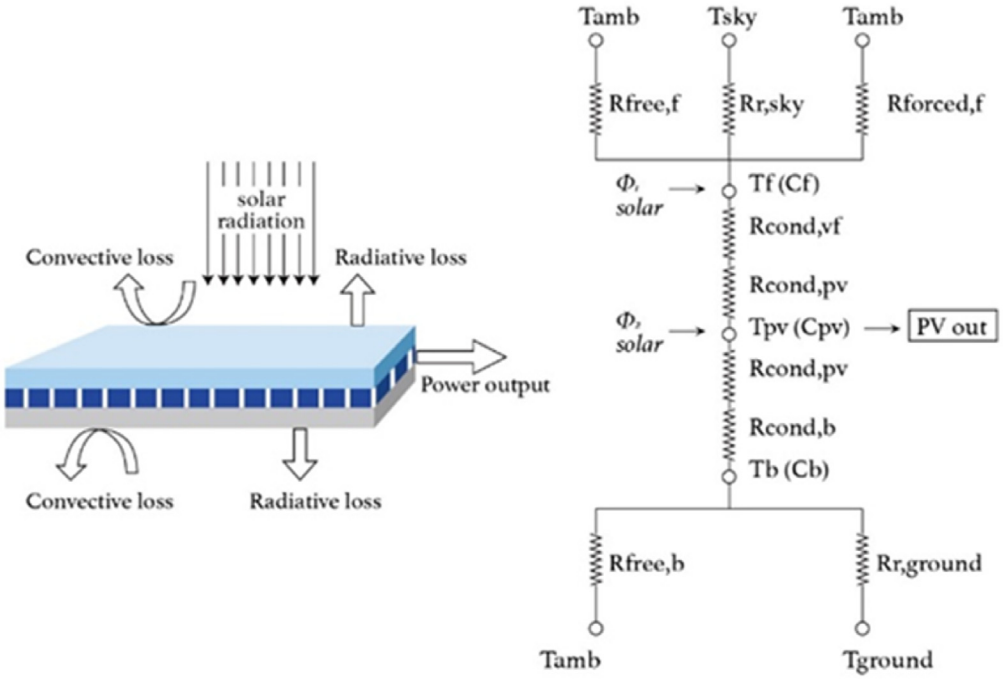

Fig. 1. Analysis of the thermal resistance of an FPV system.

models, affirming the suitability of the model for FPV panels with active water cooling.

According to Notton's model [18], each energy conservation equation for the three materials is expressed as follows:

- Front glass:

$$C_f\frac{dT_f(t)}{dt}=A_{pv}\alpha_{fg}G_g-q_{r,sky}-q_{forced,f}-q_{free,f}+q_{cond,fg-pv} \quad (1)$$

- Solar cell:

$$C_c\frac{dT_c(t)}{dt}=A_{pv}\alpha_{pv}\tau_{fg}G_g-q_{cond,f-pv}-q_{cond,b-pv}-P_{pv} \quad (2)$$

- Back Tedlar:

$$C_b\frac{dT_b(t)}{dt}=-q_{r,ground}-q_{free,b}+q_{cond,b-pv} \quad (3)$$

where T_f represents the temperature of the front glass, T_c denotes the temperature of the solar cell, T_b is the temperature of the back Tedlar, C_f represents the thermal mass of the front glass, C_c denotes the thermal mass of the solar cell, and C_b is the thermal mass of the back Tedlar. Meanwhile, $A_{pv}\alpha_{fg}G_g$ represents the radiation absorbed by the front glass, $A_{pv}\alpha_{pv}\tau_{fg}G_g$ denotes the radiation absorbed by the solar cell, $q_{forced,f}$ signifies the forced convection heat loss on the front glass, $q_{free,f}$ denotes the free convection heat loss of the front glass, $q_{free,b}$ is the free convection heat loss on the back Tedlar, $q_{r,sky}$ represents the radiation heat loss on the front glass to the sky, $q_{r,ground}$ denotes the radiation heat loss on the back Tedlar to the ground, $q_{cond,f-pv}$ is the conduction heat transfer from the front glass to the pv panel, and $q_{cond,b-pv}$ is the conduction heat transfer from the pv panel to the back Tedlar. Throughout this study, the units in the equation adhere to the International System of Units (SI units).

2.2. Thermal and physical properties of solar panels

(1) Conversion efficiency [18]

The precise conversion efficiency should consider the modification by the temperature coefficient β and irradiance coefficient γ. The relationship is expressed as follows:

$$\eta_c=\eta_{ref}[1-\beta_{ref}(Tc-T_{ref})+\gamma\, log_{10}I(t), \quad (4)$$

where η_{ref} denotes the efficiency under standard test conditions (STC), β_{ref} is the temperature coefficient (−0.0048) [21], γ represents the irradiance coefficient (0.12), Tref represents temperature under STC condition, (25 °C), and I(t) represents current generated with respect to time.

(2) Solar radiation absorbed by the panels [18]

Solar radiation is first absorbed by the first layer of glass, a high-transmittance material to the maximum incident solar radiation. The transmitted solar radiation is then absorbed by the solar cell for energy conversion.

$$Front\ glass: G_1=\alpha_{fg}\times G_g, \quad (5)$$

$$Solar\ cell: G_2=\alpha_{pv}\times\tau_{fg}\times G_g, \quad (6)$$

where G_g denotes the solar radiation, α_{fg} represents the absorptivity of the front glass (0.04), τ_{fg} is the transmittance of the front glass (0.9), and α_{pv} is the absorptivity of the solar cell (0.87) [18].

(3) Thermal mass of the solar panels

Thermal mass is essential for thermal analysis, representing the capacity for storing energy within a material. Therefore, thermal mass plays a role in resisting temperature fluctuations and introduces a time delay for temperature changes in varying conditions. The thermal mass of the solar panels C_{module} is computed based on the physical properties of each layer of material, expressed as:

$$C_{module}=\sum_m A\times d_m\times\rho_m\times C_m, \quad (7)$$

where A is the area of the solar panels, d_m is the thickness of the material, and ρ_m is the density of the material, C_m is the thermal mass of each layer of the solar panel.

(4) Physical properties of each layer of a solar panel (Table 1)

To calculate the temperature through thermal analysis, the physical properties of the PV panels must be provided. Armstrong [22] outlined the

Table 1. Physical properties of each layer of the solar panels.

Layer	Thickness (mm)	Thermal conductivity (W/mK)	Density (kg/m^3)	Specific heat capacity (J/kg°C)
1. Glass	3.2	1.8	3000	500
2. ARC	1×10^{-5}	32	2400	691
3. PV cells	0.3	148	2330	677
4. EVA	0.05	0.35	960	2090
5. Tedlar	0.5	0.2	1200	1250

properties of materials in different layers (Table 1). The PV panels typically comprise five main layers: glass covering, anti-reflective coating (ARC), PV cells, ethylene vinyl acetate (EVA) layer, and a Tedlar PVF layer. Considering the relevant heat transfer theory [18], PV cells can be categorized into three parts: front glass, solar cell, and back Tedlar. The heat transfer effect of ARC can be disregarded due to its relatively small dimension and specific heat capacity compared to other components. EVA is considered a part of the solar cell, enabling its calculation to be integrated with that of the solar cell.

2.3. Calculation of the heat transfer on the boundaries of the PV panels

(1) Free convection

The free convection between the panels and air can be divided into two parts: the front panel and the back panels. The convection coefficient is expressed as follows:

$$q_{free} = A_{pv} \cdot h_{free} \cdot \left[T_{pv} - T_{amb}\right], \tag{8}$$

$$h_{free} = \frac{k_a Nu}{L}, \tag{9}$$

where q_{free} represents the free convection heat transfer, A_{pv} denotes the area of the PV panels, h_{free} is the free convection coefficient, T_{pv} represents the temperature of the PV panels, T_{amb} is the temperature of ambient air, k_a is the thermal conductivity of air, L is the length of the PV panels, and Nu is the Nusselt number, according to Holman [23]. The Nusselt number for the inclined plane is derived as follows:

Free convection on the front panels [23]:

$$Nu = 0.14\left[(GrPr)^{\frac{1}{3}} - (Gr_c\, Pr)^{\frac{1}{3}}\right] + 0.56[GrPr\cos(90^\circ - \theta)]^{1/4} \tag{10}$$

Free convection on the back panels :

$$Nu = 0.56[GrPr\cos(90^\circ - \theta)]^{1/4} \tag{11}$$

where Ra is the Rayleigh number, Pr is the Prandtl number, Gr is the Grashof number, Gr_c is the critical Grashof number, and θ is the incline angle of the PV panels. Equations (10) and (11) are valid for θ between 15 and 75°.

(2) Forced convection for the front panels

When wind flows through the front surface of the PV panels, the air cools the panels down via force convection heat transfer. As used by Armstrong et al. [22], the heat transfer coefficient is derived as the flow through the inclined plane:

$$q_{forced} = A_{pv} \cdot h_{forced} \cdot \left[T_{pv} - T_a\right], \tag{12}$$

$$Nu = 0.037 Re^{4/5}\, Pr^{1/3} \tag{13}$$

where q_{forced} denotes the forced convection heat transfer, h_{forced} is the forced convection coefficient, Re is the Reynolds number ($\rho VD/\mu$), and Nu represents the Nusselt number [18].

(3) Radiation heat transfer for PV panels

Radiation heat involves the emission of electromagnetic waves based on the body's temperature. The radiation heat exchange between the PV panels and the environment is divided into two components: the front panels with the sky and the back panels with the ground. The heat transfer rate and the shape factor were previously presented by Liu and Jordan [24] and are expressed as follows:

$$q_{rad\_f} = A_{pv}\sigma\left[\varepsilon_{pv} \cdot T_{pv}^4 - F_{f,sky}\varepsilon sky \cdot T_{sky}^4\right], \tag{14}$$

$$F_{f,sky} = \frac{1}{2}(1 + \cos\theta), \tag{15}$$

$$q_{rad\_b} = A_{pv}\sigma\left[\varepsilon_{pv} \cdot T_{pv}^4 - F_{b,gr}\varepsilon_{gr} \cdot T_{gr}^4\right], \tag{16}$$

$$F_{b,gr} = \frac{1}{2}[1 - \cos(\pi - \theta)], \tag{17}$$

where q_{rad_f} is the radiation heat transfer on the front surface, σ is the Stefan−Boltzmann constant, F is the shape factor, εsky is the emissivity of the sky, and ε_{gr} is the emissivity of the ground.

(4) Water spray cooling heat transfer

The active cooling of a water spray removes heat from the back surface of the PV panels. The following empirical formula was developed by Oliphant [25]:

$$q_{spray} = A_{spray} \cdot h_{spray} \cdot \left[T_{pv} - T_w\right], \tag{18}$$

$$h_{spray} = \frac{k_w Nu}{D}, \tag{19}$$

$$Nu = 32.5(Re^*)^{0.51}, 10 \le Re^* \le 1000 \tag{20}$$

$$Re^* = \frac{GD}{\mu_w}, G = \frac{\dot{m}}{A_{sp}}, D = 2H_{sp} \cdot tan(0.5\gamma),$$

where q_{spray} is the water spray cooling heat transfer, A_{spray} is the area of the water spray, h_{spray} is the heat transfer coefficient of the water spray, T_w is the temperature of the cooling water, k_w is the conductivity of the water, H_{sp} is the distance from the water spray outlet to the PV panel, and D is the spray diameter on the PV panel.

(5) Water film cooling heat transfer

The PV panels employ water film cooling, and its heat transfer is similar to water flowing through a plate. According to Schiro et al. [26], the formula is presented as follows:

$$q_{film} = A_{pv} \cdot h_{film} \cdot \left[T_{pv} - T_w\right], \tag{21}$$

$$h_{film} = \frac{k_w Nu_L}{D}, \tag{22}$$

$$Nu_L = 0.664\, Re_L^{\frac{1}{2}} Pr^{\frac{1}{3}}, \tag{23}$$

$$Re_L = \frac{\rho u_\infty L}{\mu}, yc = \sqrt[3]{\frac{Q^2}{gB^2}}, u_\infty = \frac{Q}{A} = \frac{Q}{y_c B}.$$

2.4. Clearness index

To compare the experiment results under similar conditions, this study employed the clearness index to differentiate the solar radiation condition affected by the cloud [27]. GHI stands for global horizontal irradiation, which is measured by a pyranometer. GHI_{clear} represents the radiation during a clear sky, calculated using a declination angle, the hour angle of the sun, and the longitude and latitude coordinates of the site. For a clearness index exceeding 0.75 (Table 2), the sky condition is categorized as a clear sunny day, and this value is the preferred interval for the experiment.

$$clearness\ index\ (Kt) = \frac{GHI}{GHI_{clear}}. \tag{24}$$

Table 2. Different radiation conditions distinguished by calculating the clarity [27,28].

Sky condition	Clearness index (Kt)
Cloudy	0−0.2
Partly cloudy	0.2−0.6
Partly Sunny	0.6−0.75
Sunny	0.75−1

2.5. Cost-effectiveness evaluation

Two parameters were employed to evaluate the economic viability of the FPV system in this study: the levelized cost of energy (LCOE) and the payback period (PP). LCOE is a measure of lifetime cost divided by energy production, offering an economic assessment of the present value of the unit cost of electricity. The lifetime cost encompasses several factors, including investment, operational and maintenance expenses, and fuel costs, among others. The following equation calculates the LCOE:

$$LCOE = \frac{\sum_{t=1}^{n} \frac{I_t + M_t}{(1+r)^t}}{\sum_{t=1}^{n} \frac{E_t}{(1+r)^t}} \tag{25}$$

where t represents the year, I_t is the investment cost in the year t, M_t is the operational and maintenance cost of the system in the year t, E_t is the electricity production, n is the lifetime of the system, and r is the discount rate. In the system employed in this study, the investment cost referred to the cost of the solar system and installation. Operational and maintenance costs were represented by the annual expenditure of the system maintenance. It can be calculated that the LCOE of the system in this study is \$155/MWh by setting the discount rate of 4% [29].

PP is another parameter that can be utilized to evaluate the time to recoup the initial investment of the system. It can be calculated as follows:

$$PP = \frac{ln\left(\frac{1}{1 - \frac{I_{t=1} \times r}{CF}}\right)}{ln\,(1+r)} \tag{26}$$

where $I_{t=1}$ is the initial cost of the system and CF is the cash flow of each year. It can be calculated that the PP of the system employed in this study is 7.56 years [29].

3. Experimental investigation

3.1. Experimental process and configuration

A 265 W solar panel was installed tilted on the experimental constant temperature water tank, as shown in Fig. 2. The water temperature was kept constant at 25 °C by regulating the water flow rate from the geothermal cooling water. This choice of water temperature to be 25 °C was based on its convenience for experimental control and ensuring that the experimental results were not influenced by

this factor. Additionally, this temperature aligns with STC temperature. The water-cooling system incorporated a water spray on the back side and a water film on the front. A 20 W temperature-controlled pump facilitated flow for the cooling system. The experiment aimed to compare the efficiency of floating solar panels with that of rooftop solar panels and evaluate the impact of using active cooling on floating solar panels.

The experiment was conducted on a whole day in Yilan, Taiwan, on a sunny summer day to ensure sufficient radiation for comparison and experimental procedures. Fig. 3 illustrates the flowchart of the experimental process. Before the experiment started, theoretical analysis and a short-time data validation were conducted to establish the PV system model for the experiments. Subsequently, the experiment was divided into three parts. In the first experiment, the cooling system was deactivated to compare the floating solar panels with the rooftop solar panels. This segment measured the temperature and efficiency differences of the solar panels attributed to the cooling effect of the water tank. In the second experiment, the water spray cooling method was implemented. The pump operated the cooling system, spraying the cooling water at the back side of the solar panels using eight uniformly distributed nozzles. The pump was triggered once the panel temperature reached 45 °C, with the switch-off temperature calculated to optimize the net output. This process was repeated throughout the entire experiment period to compare the difference in net power output between the water spray active cooling floating solar panels and the rooftop panels. In the third experiment, a pump was used to operate the water film cooling systems. A pipe with uniformly distributed holes generated a smooth water film to flow over the front side of the panels. The pump also adopted temperature control to gain the maximum power output for comparison with the rooftop panels.

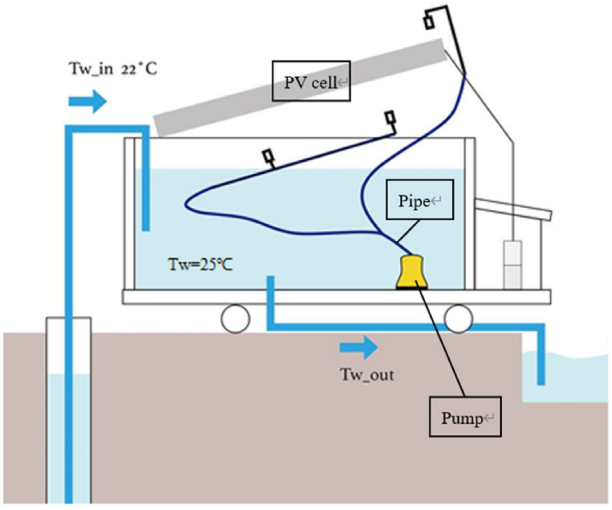

Fig. 2. Schematic diagram of the simulated FPV experimental system.

3.2. Experimental equipment

Anji Technology manufactured the 265 W polycrystalline solar panels, which measured 1632 mm × 995 mm × 40 mm. The solar panels were installed at tilts of 18° and 40° southwest, as shown in Fig. 4. The independent solar systems were connected to the Morningstar Sunsaver MPPT to transfer electric currents to the batteries and record the power output

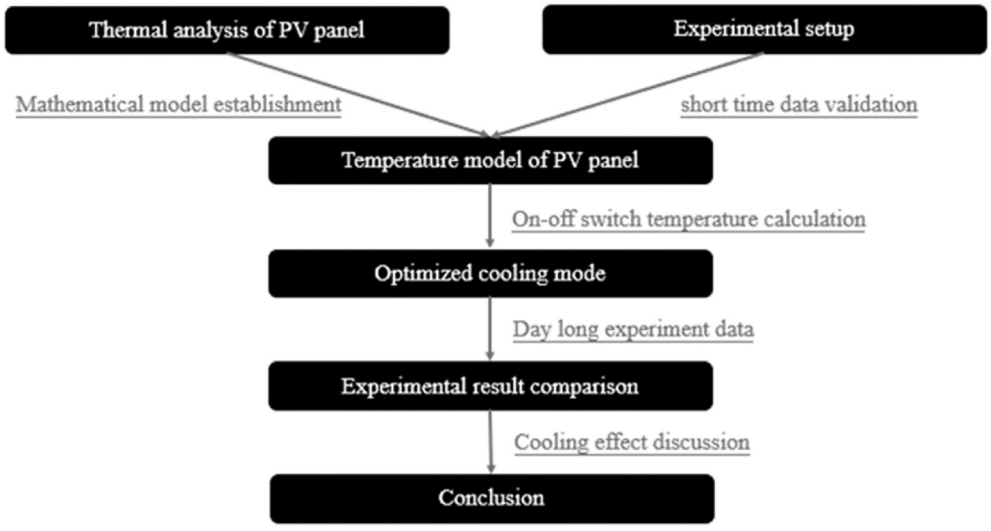

Fig. 3. Experimental process.

of the solar panels. The maximum current capacity was 15 A, and the power measurement accuracy was ±2%. The cooling system included a 2 m × 1.4 m × 0.7 m water tank and a diaphragm pump with a 25 lpm max flow rate and nozzles. Temperature measurement utilized a T-type thermocouple, with an error range of ±0.5 °C within a temperature range of "0 °C < T < 200 °C" and an accuracy of ±0.2 °C. Wind speed and ambient temperature were measured by the TESTO 480 climate measuring instrument, generating an accuracy of ±0.03 m/s and ±0.5 °C, respectively. Solar radiation was measured by the LP-PYRA12 pyranometer with a spectral selectivity of ±18W/m^2. To visualize the temperature distribution of the solar panels, the experiment also used the infrared thermal imaging camera FLIR E63900 with an accuracy of ±2% or 2 °C. The detailed specification of the PV cell used in the experiment is outlined in Table 3.

4. Results and Discussion

The results of this study are divided into two parts: 1) a brief 1-hour experiment aimed at validating the accuracy of the solar panel temperature model and 2) a whole-day experiment discussing the energy gain enhancement by comparing the net power output of each experiment. The experiment was conducted from June 20 to June 28. Part 1 aims to make the experiments more realistic and closer to actual conditions. Thus, the experiment was conducted in an actual environment. To closely match environmental conditions, this study chose the place and time closest to the STC condition and the same irradiation.

4.1. Validation of the calculation of the solar panel temperature

The first experiment was conducted from 9:32 am to 10:55 am, during which the radiation fluctuated between 400 and 700 W/m^2, and wind speeds ranged from 0.5 to 3 m/s, as shown in Figs. 5 and 6. The average ambient temperature was 33 °C throughout the experimental period. Notably, the mathematical model adeptly captured the temperature fluctuation during rapid radiation and weather changes. The RMSE stood at 0.97 °C, with a thermal calculation error of 11.64%. The results affirm the suitability of the temperature model derived through thermal analysis for floating solar panels (Fig. 7).

In the second experiment, water film cooling was applied on floating solar panels. During the experimental period, the solar panels remained operational from 10:52 am to 11:15 am amidst varying radiation levels of 800−1000 W/m^2 and wind speeds of 0.5−2 m/s, as shown in Figs. 8 and 9. The average ambient temperature was 33 °C.

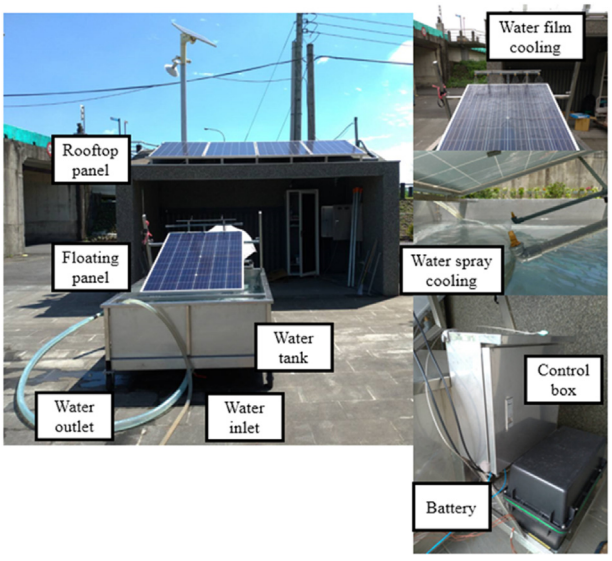

Fig. 4. Structure of the installed FPV system.

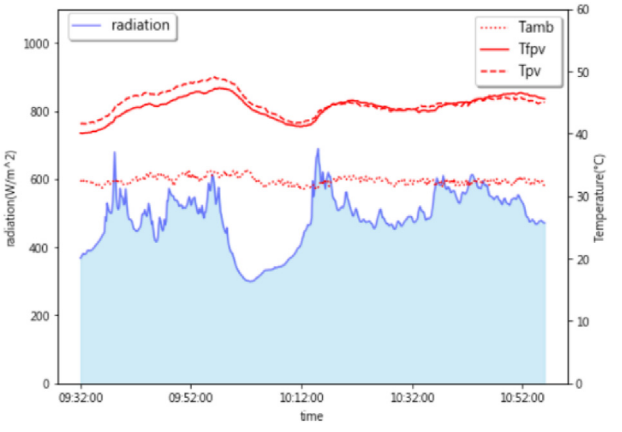

Fig. 5. Radiation and FPV panel temperature in the experiment without cooling.

Table 3. Specification of the PV cell.

Maximum power	Open circuit voltage Voc	Short circuit current Isc	Maximum power voltage Vmpp	Maximum power current Impp
265W	38.65V	9.14A	31.52V	8.41A

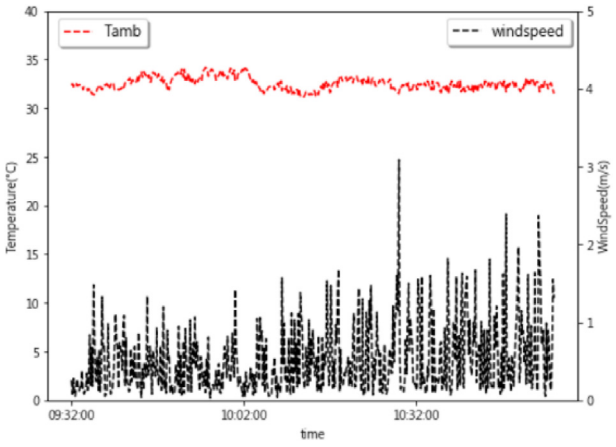

Fig. 6. Wind speed and ambient temperature in the experiment without cooling.

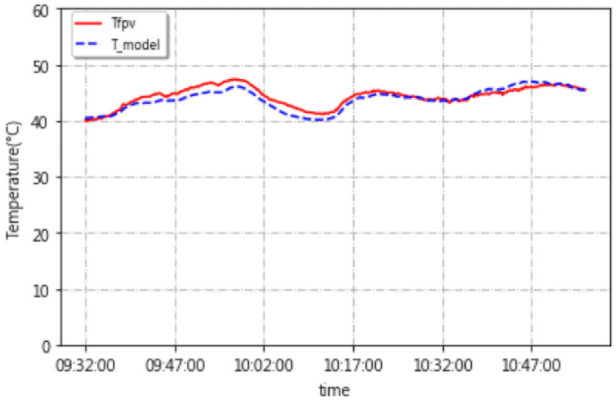

Fig. 7. Model calculation of the FPV panels with radiation changes in the experiment without cooling.

The experiment was structured into three cooling periods for mathematical validation. Fig. 10 illustrates the time delay observed in temperature changes on the back panels due to water film

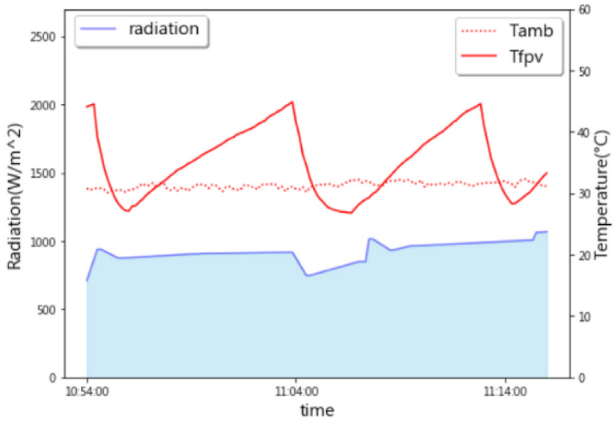

Fig. 8. Radiation and FPV panel temperature in the experiment of water film cooling.

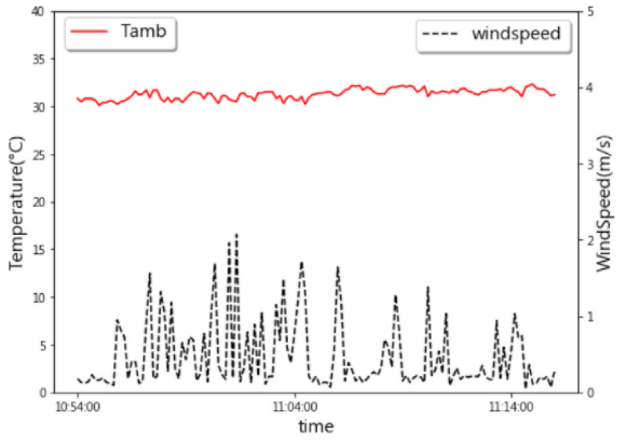

Fig. 9. Wind speed and ambient temperature in the experiment of water film cooling.

cooling applied on the front panels. The mathematical model accounts for this time delay by considering the thermal mass and heat transfer rate in each layer of the solar panels. The model demonstrated an RMSE of 2.36 °C, with a thermal calculation error of 11.31%.

In the third experiment, water spray cooling was applied on the back panels. The experiment was conducted from 13:00 pm to 14:10 pm to 2:10 pm, with steady radiation levels at about 900 W/m^2 throughout the experimental period, accompanied by wind speeds ranging from 0.5 to 3 m/s, as shown in Figs. 11 and 12. The average ambient temperature was 35 °C. Fig. 13 illustrates the temperature change of the water spray cooling during the experimental period. Remarkably, the experimental result closely aligns with the proposed model, showcasing a slightly lower temperature on the back surface than on the front surface. The model yielded an RMSE of 1.71 °C, with a thermal calculation error of 14.68%.

4.2. Enhancement of energy gain on solar panels by applying different cooling methods

The first experiment was conducted from 12:49 pm to 16:00 pm. During the 3-hour period, the average ambient temperature was 30 °C, while the average solar radiation was 800 W/m^2, as shown in Fig. 14. The maximum ambient temperature and solar radiation peaked at 13:00 pm, leading to the maximum temperature difference between the floating and rooftop panels. The cell temperature registered 68.7 °C for the rooftop panels and 62 °C for the floating panels. These results underscore the cooling effects of the floating panels and reveal that the high cell temperature of over 60 °C at noon in

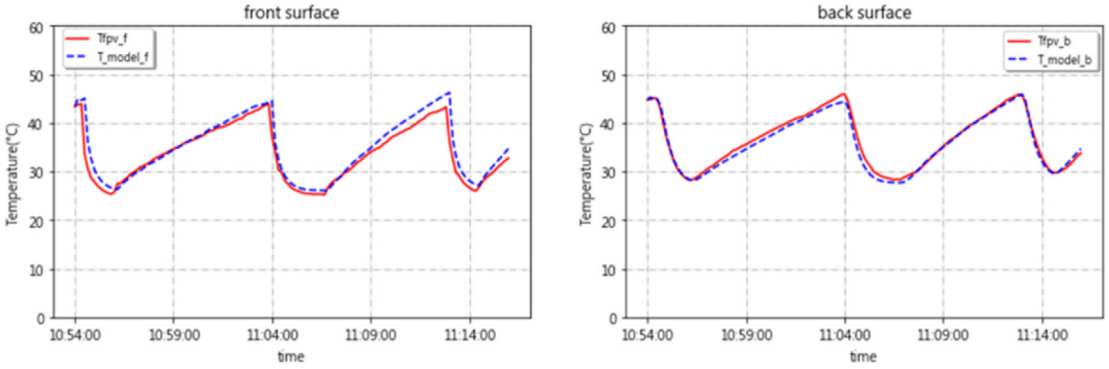

Fig. 10. The isothermal model calculates the temperature of the FPV panels with water film cooling on the front panel: (a) front panel and (b) back panel.

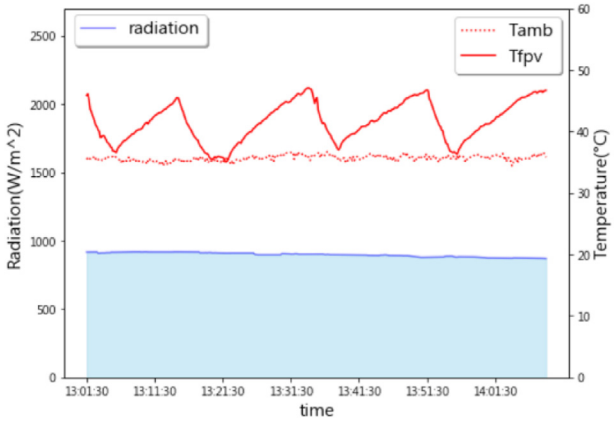

Fig. 11. Radiation and FPV panel temperature in the experiment of water spray cooling.

summer requires other active cooling methods are necessary to avoid efficiency drop.

To facilitate a comparative analysis under similar weather conditions, as shown in Fig. 15,

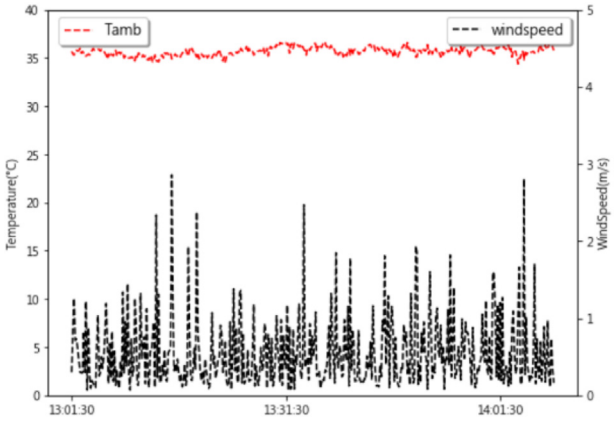

Fig. 12. Wind speed and ambient temperature in the experiment of water spray cooling.

the data was filtered using a clearness index above 0.75. Under these conditions, the average cell temperature recorded was 59.7 °C for the rooftop panels and 55.7 °C for the floating panels, indicating a 4 °C temperature differential and a 3.27% increase in average power generation. These results indicate that the cooling effect of the floating panels positively affects conversion efficiency.

The second experiment applied water film cooling on the floating panels. The experiment was conducted from 11:00 am to 16:00 pm. During the 5-hour experiment, the ambient temperature ranged from 33 to 38 °C, with the maximum solar radiation peaking at 1125 W/m^2 at 13:25 pm. As shown in Fig. 16, the cooling system operated intermittently, regulating the cell temperature of the floating panels with water film cooling between 31 °C and 45 °C. Comparing the cell temperature behavior with and without the cooling system, the average cell temperature with a cooling system was 37.4 °C, and the cell temperature without cooling was 55.6 °C. The average cooling effect of 18 °C led to a 6.7% power enhancement, as shown in Fig. 17. After factoring in the energy consumption associated with pumping the cooling system, the net efficiency increase was calculated at 5.3%.

In the third experiment, water spray cooling was applied on the floating panels. The experiment was conducted from 11:00 am to 14:00 pm. During the 3-hour experiment, the ambient temperature was 35 °C, while the radiation ranged from 800 to 920 W/m2. Fig. 18 illustrates the on-off cycling of the cooling system, with longer cooling periods attributed to the lower cooling capacity of the water spray. Through optimization calculations, the cell temperature was controlled between 37 °C and

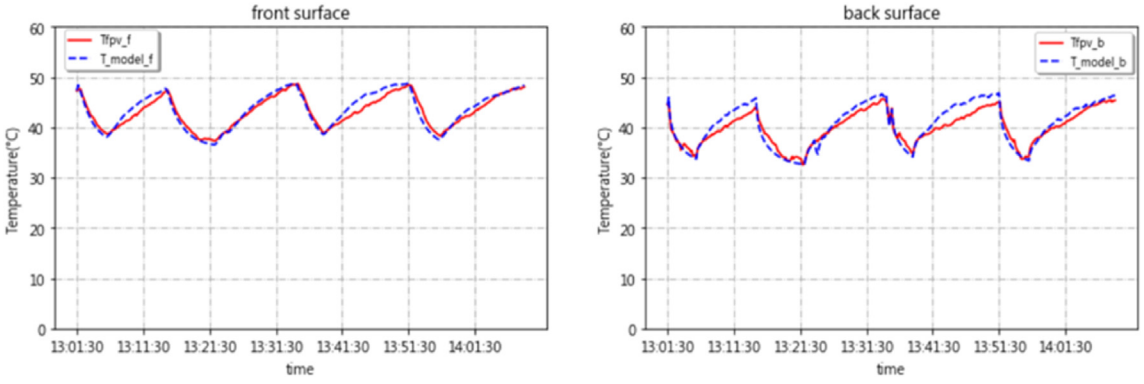

(a) (b)

Fig. 13. Temperature model of the FPV panels sprayed on the back panel: (a) front panel and (b) back panel.

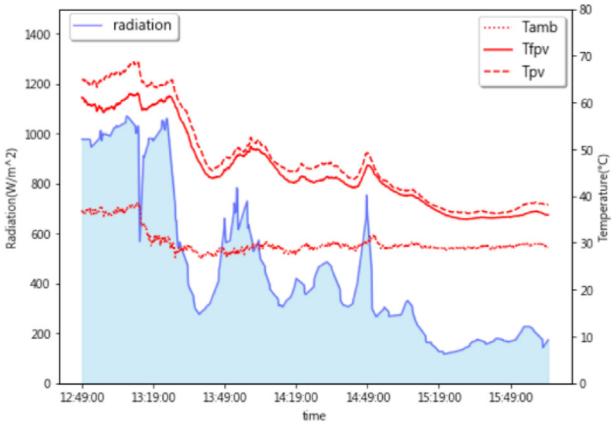

Fig. 14. Solar radiation and FPV panel temperature.

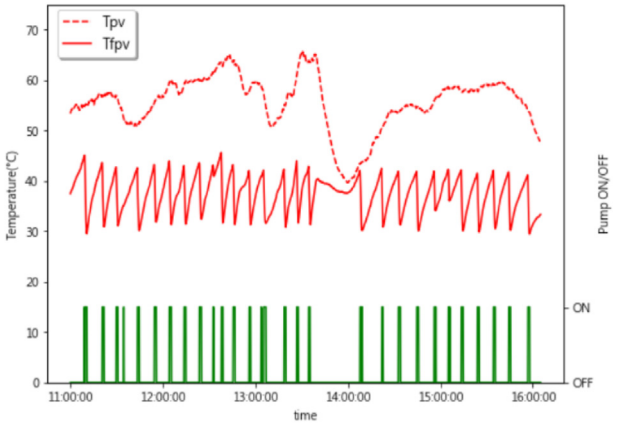

Fig. 16. The cooling system start and stop, and the solar panel temperature.

45 °C. During the experiment, the average cell temperature was 43.4 °C for the floating panels with water spray cooling and 59.7 °C for those without cooling. This substantial 16.3 °C temperature difference led to a 6.38% power increase. Accounting for energy consumption by the cooling system, the net power gain was calculated at 3.93%, as shown in Fig. 19.

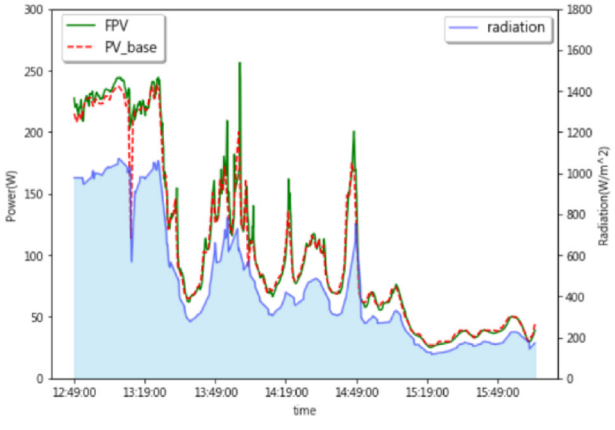

Fig. 15. Comparison of FPV and rooftop PV generation.

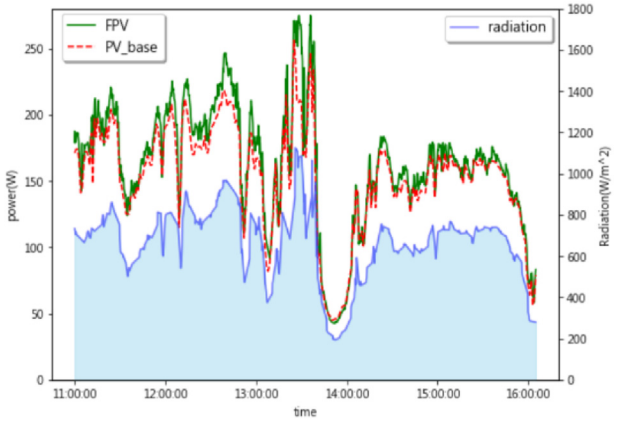

Fig. 17. Comparison of the front panel water film cooling and rooftop PV generation.

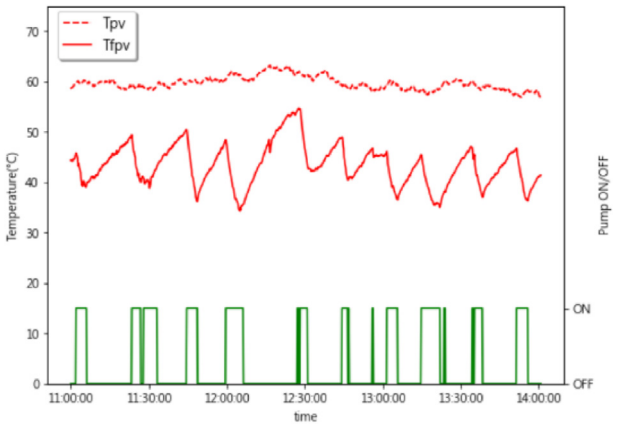

Fig. 18. Start and stop of the back panel spray cooling system and the solar panel temperature.

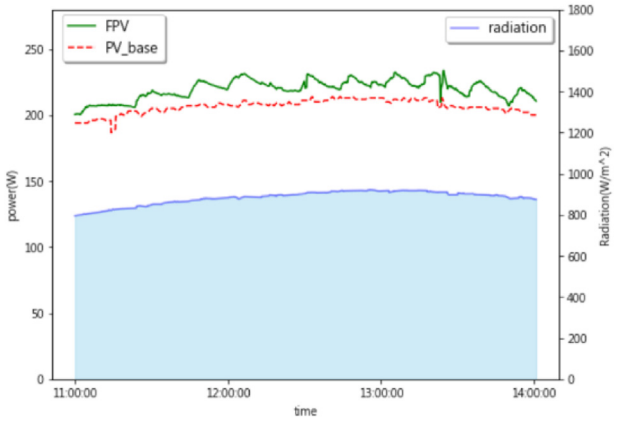

Fig. 19. Comparison of FPV back spray cooling and rooftop PV generation.

5. Conclusions

This study provides valuable insights into the cooling effect of floating solar panels and the application of active cooling methods in subtropical regions. The results confirmed that the conversion efficiency of solar panels decreases as the cell temperature increases and that applying active cooling significantly affects the cell temperature. The net power gain could be increased by optimizing the cooling pattern. Moreover, a mathematical model was derived to fit the cell temperature of the solar panels under different cooling conditions. The key conclusions drawn from the research are as follows:

(1) The temperature model derived from energy conservation equations accurately predicts the cell temperature of solar panels in different cooling conditions. Validated by experimental data, the RMSE is 0.97 °C for passive cooling on floating solar panels, 2.36 °C for water film cooling on floating solar panels, and 1.71 °C for water spray active cooling on floating solar panels. These results affirm the accuracy of the thermal analysis of the solar panels and the cooling methods. Since the temperature model is derived from physical properties, the model can be used in a different area for estimation.

(2) During the whole-day experiment in summer, the floating solar panels recorded a 4.03 °C lower cell temperature than the rooftop panels, leading to a 3.27% higher power gain.

(3) The economic analysis of the FPV system can be evaluated using LCOE and PP. The LCOE of FPV in this study is $155/MWh, while PP is 7.56 years.

(4) Applying water-cooling techniques on floating solar panels is feasible, as it benefits from the high accessibility of a cooling water source with a steady temperature. Based on the experimental results, water film cooling could lower the average temperature of PV panels by 19.39 °C and increase the net power output by 5.27%. Moreover, water spray cooling could lower the average temperature of PV panels by 16.29 °C and increase the net power output by 3.93%.

Ethical statement

Ethical approval was not applicable for the present study because this study did not involve human or live animal experiments.

Conflicts of interest

The authors declare no issues related to conflicts of interest involved in this manuscript.

Acknolowledgments

The authors gratefully acknowledge the financial and technical support provided by contract No. 105-2627-M-001 -013 offered by Ministry of Science and Technology and Bureau of Energy, Ministry of Economic Affairs, Taiwan, R. O. C.

References

[1] Ranjbaran P, Yousefia H, Gharehpetian GB, Astaraei FR. A review on floating photovoltaic (FPV) power generation units. Renew Sustain Energy Rev 2019;110:332−47.
[2] Sinke WC. Development of photovoltaic technologies for global impact. Renew Energy 2019;138. 991-914.
[3] Stiubiener U, Carneiro da Silva T, Trigoso FBM. PV power generation on hydro dam's reservoirs in Brazil: A way to improve operational flexibility. Renew Energy 2020;150: 765−76.
[4] Dai J, Zhang C, Lim HV, Ang KK, Qian X, Wong JLH, Tan ST, Wang CL. Design and construction of floating modular

photovoltaic system for water reservoirs. Energy 2020;191: 116549.
[5] Oliveira-Pinto S, Stokkermans J. Assessment of the potential of different floating solar technologies: Overview and analysis of different case studies. Energy Convers Manag 2020; 211.
[6] Sahu A, Yadav N, Sudhakar K. Floating photovoltaic power plant: A review. Renew Sustain Energy Rev 2016;66:815−24.
[7] Choi YK. A Study on Power Generation Analysis of Floating PV System Considering Environmental Impact. Int J Softw Eng Appl 2014;8(1):75−84.
[8] Umoette AT. Design of Stand Alone Floating PV System for Ibeno Health Centre. Sci J Energy Eng 2016;4(6):56−61.
[9] Chandela SS, Agarwalb T. Review of cooling techniques using phase change materials for enhancing efficiency of photovoltaic power systems. Energy Convers Manag 2017;73: 1342−51.
[10] Azmi MSM, Othman MYH, Ruslan MHH, Sopian K, Majid ZAA. Study on electrical power output of floating photovoltaic and conventional photovoltaic. AIP Conf Proc 2013;1571:95−101.
[11] Cazzaniga R, Rosa-Clot M, Rosa-Clot P, Tina GM. Floating tracking cooling concentrating (FTCC) systems. In: Paper presented at: the 2012 38th IEEE photovoltaic specialists conference; 2012 (Austin, TX).
[12] Nisar H, Janjua AK, Hafeez H, Shakir S, Shahzad N, Waqas A. Thermal and electrical performance of solar Floating PV system compared to on-ground PV system-an experimental investigation. Sol Energy 2022;241:231−47.
[13] Dorobantu L, Popescu MO. Increasing the efficiency of photovoltaic panels through cooling water film. Sci Bull, Series C 2013;75(4):223−32.
[14] Nižetić S, Čoko D, Yadav A, Grubišić-Čabo F. Water spray cooling technique applied on a photovoltaic panels: The performance response. Energy Convers Manag 2016;108:287−96.
[15] Akhsassi M, Fathi AE, Erraissi N, Aarich N, Bennouna A, Raoufi M, Outzourhit A. Experimental investigation and modeling of the thermal behavior of a solar PV module. Sol Energy Mater Sol Cell 2018;180:271−9.
[16] Jones AD, Underwood CP. A thermal mode for photovoltaic systems. Sol Energy 2001;70:349−59.
[17] Hameed RH. Mathematical Model to Investigate the Temperature. J Univ Babylon Eng Sci 2018;26.
[18] Notton G, Cristofari C, Mattei M, Poggi P. Modelling of a double-glass photovoltaic module using finite differences. Appl Therm Eng 2005;25(17−18):2854−77.
[19] Asdrubali F, Evangelisti L, Grazieschi G, Guattari C. Influence of sky temperatures on building energy needs. In: Proceedings of building simulation 2019: 16th conference of IBPSA; 2019. p. 293−9.
[20] International Organization for Standardization. Energy performance of buildings - calculation of energy use for space heating and cooling. Geneva: ISO; 2007. ISO 13790:2007.
[21] Evans DL. Simplified method for predicting photovoltaic array output. Sol Energy 1981;27(6):555−60.
[22] Armstrong S, Hurley WG. A thermal model for photovoltaic panels under varying atmospheric conditions. Appl Therm Eng 2010;30(11−12):1488−95.
[23] Holman JP. Heat transfer. eighth ed. New York: McGraw Hill; 1997.
[24] Liu BYH, Jordan RC. The long-term average performance of flat-plate solar-energy collectors: With design data for the U.S., its outlying possessions and Canada. Sol Energy 1963; 7(2):53−74.
[25] Oliphant K, Webb BW, McQuay MQ. An Experimental Comparison of Liquid Jet Array and Spray Impingement Cooling in the Non-boiling Regime. Exp Therm Fluid Sci 1998;18(1):1−10.
[26] Schiro F, Benato A, Stoppato A, Destro N. Improving photovoltaics efficiency by water cooling: Modelling and experimental approach. Energy 2017;137:798−810.
[27] Collares-Pereira M, Rabl A. The average distribution of solar radiation-correlations between diffuse and hemispherical and between daily and hourly insolation values. Sol Energy 1979;22(2):155−64.
[28] Mukkavilli SK. Investigating Australian dust aerosol spatiotemporal effects on direct normal irradiance forecasts. [dissertation]. Sydney(AU): The University of New South Wales; 2018.
[29] Sutanto B, Iacovides H, Nasser A, Cioncolini A, Afgan I, Indartono YS, Prasetyo T, Wijayanta AT. Appl Therm Eng 2024;236 part D:121801.